Advanced Functional Materials

ADVANCED FUNCTIONAL MATERIALS
www.afm-journal.de

RESEARCH ARTICLE OPEN ACCESS

A Host-Guest, Zeolite/Organocation Material With Isotropic Zero Thermal Expansion

João Pedro Falk de Campos[1] | Erik Elkaim[2] | Meng He[3] | Bruno Alonso[1] | Julien Haines[1]

[1]Institut Charles Gerhardt Montpellier, CNRS, ENSCM, Université de Montpellier, Montpellier, France | [2]Synchrotron SOLEIL, Saint-Aubin, France | [3]European Synchrotron Radiation Facility, Grenoble, France

Correspondence: Bruno Alonso (bruno.alonso@umontpellier.fr) | Julien Haines (julien.haines@umontpellier.fr)

Received: 9 February 2026 | **Revised:** 23 March 2026 | **Accepted:** 28 March 2026

Keywords: host-guest | x-ray diffraction | zeolite | zero thermal expansion

ABSTRACT

The thermal expansion of the host-guest material, siliceous chabazite- N,N,N-trimethyl-1-adamantyl ammonium, (CHA-TMAda), obtained directly from hydrothermal synthesis, and calcined siliceous chabazite (CHA) were measured by variable-temperature, high-resolution, synchrotron, x-ray powder diffraction. In contrast to the strong negative thermal expansion (NTE) found for chabazite, CHA-TMAda exhibits isotropic zero thermal expansion (ZTE) with one of the lowest, measured, volume thermal expansion coefficients (α_v) of $0.12(2) \times 10^{-5}$ K^{-1} from 120–394 K. This striking result is due to the presence of TMAda in the large chabazite cages of CHA and fluoride ions in the double six-membered rings that strongly reduce transverse displacements of the oxygen atoms in the CHA framework, which are linked to the NTE mechanism in CHA. The use of selected organic structure directing agents, as in this case TMAda, for the hydrothermal synthesis of targeted zeolites provides a straightforward strategy to obtain a new class of host-guest, nanostructured, crystalline ZTE materials made of light and abundant elements.

1 | Introduction

Zero thermal expansion (ZTE) materials are of great technological interest due to their potential use in mechanical, electronic, thermal, optical and aerospace applications [1–21]. These materials [15] are characterized by linear thermal expansion coefficients $|\alpha_l|$ of less than 0.1×10^{-5} K^{-1}, corresponding for a cubic material to a volume coefficient $|\alpha_v|$ of less than 0.3×10^{-5} K^{-1}. ZTE materials are often obtained by combining materials exhibiting positive and negative thermal expansion (NTE) to form composites with low or zero thermal expansion. Such composites present a drawback as they are subject to cracking due to the difference in thermal expansion of the two components. Relatively few ZTE materials have been identified including metallic alloys [4] (INVAR-FeNi36, Fe-33Ni-4.5Co and related systems), the vitroceramic composite ZERODUR [1], and framework structures [2, 7, 8, 10, 11, 13–17, 18, 21] such as $Sc_{1.5}Al_{0.5}W_3O_{12}$ [15], $(LiFe)_{0.5}xCu_{2-x}V_2O_7$ [18] and $K_xMn_xIn_{2-x}(MoO_4)_3$ based materials [21]. In this context, the concept of average atomic volume (AAV) [22] has proved to be useful to design such materials as it has been observed that a critical value of 16 $Å^3$ exists corresponding to ZTE, with higher values corresponding to systems exhibiting NTE and lower values positive thermal expansion (PTE). The variation in the amount of space around atoms provides a mechanism to modulate the low-energy vibrations responsible for NTE in framework structures. However, many of the above materials contain transition metals and/or technology-critical elements. Most are materials with properties that can be tuned by chemical composition, such as alloys, solid solutions, and vitroceramic composites. Single component materials exhibiting intrinsic ZTE properties present advantages in terms of preparation and stability. The framework material, $Sc_{1.5}Al_{0.5}W_3O_{12}$, for example, presents ZTE over a very large temperature range from 4–1400 K.

An alternative strategy to attain ZTE is to tune the thermal expansion properties of a porous NTE material by the insertion of guests in the pores and cages. In the family of zeotype materials, $AlPO_4$-17 exhibits the highest coefficient of negative thermal expansion $\alpha_v = -3.50 \times 10^{-5}$ K^{-1} over the 18–300 K range [23]. Typical α_v values for zeotype materials [24] lie in the range from -0.50×10^{-5} K^{-1} to -3.50×10^{-5} K^{-1}. It can be noted that these values are lower than materials which exhibit giant NTE [25], for which $\alpha_v < -5 \times 10^{-5}$ K^{-1}. The proposed NTE mechanism in $AlPO_4$-17 is linked to thermally activated transverse oxygen displacements in the Al—O—P linkages bridging the AlO_4 and PO_4 tetrahedra. This results in a reduction of the Al—O—P angles and consequently the Al—P distances in the structure yielding a contraction of the $AlPO_4$-17 framework around the empty pores and cages of the structure with increasing temperature. The very strong NTE at low temperature in $AlPO_4$-17 can be tuned by the insertion of oxygen molecules in the cages under high pressure [26]. The overall volume thermal expansion only exhibits a small change with respect to guest-free $AlPO_4$-17 at ambient pressure; however, in *a* direction, low NTE of -0.4×10^{-5} K^{-1} is observed, whereas a very strong linear NTE of -2.2×10^{-5} K^{-1} is observed in the *c* direction. These results show the strong effect of interactions with the guest molecules on the thermal expansion of the framework in the *xy* plane, which is strongly reduced.

The novel strategy investigated here to tune the thermal expansion of these frameworks is to retain the molecules that act as organic structure directing agents (OSDA) during the synthesis of these materials. The second highest α_v value among zeotypes ($\alpha_v = -2.85 \times 10^{-5}$ K^{-1} from 293–873 K) is found for siliceous chabazite [27, 28] with a closely related structure, which differs from that of $AlPO_4$-17 in the stacking sequence along *c*. The structure of chabazite (CHA, pure SiO_2, rhombohedral, space group *R*-3*m*, $a = 13.5252$ Å, $c = 14.7342$ Å) is built up of alternating double six membered rings of SiO_4 tetrahedra (*d6r*) and large chabazite cages (*cha*) along the c direction. This structure contains 4, 6, and 8-membered rings of SiO_4 tetrahedra. NTE in CHA has been linked to a thermally activated mode that translates along certain Si—O—Si—O—Si linkages in the *d6r* resulting in a reduction in Si-Si distances [29]. Pure silica CHA can be synthesized by hydrothermal methods using N,N,N-trimethyl-1-adamantyl ammonium ions (TMAda) [27] as the OSDA. In the present study, the thermal expansion properties of this material, CHA-TMAda, directly obtained from hydrothermal synthesis, are investigated by high-resolution, synchrotron, x-ray powder diffraction (XRPD) in order to determine the effect of the presence of TMAda in the large *cha* cages and fluoride ions in the *d6r* as compared to guest-free, calcined CHA with its strong intrinsic NTE.

2 | Results and Discussion

CHA-TMAda and CHA were studied by XRPD over the 120–394 K and 100–1008 K ranges, respectively. Full structure refinements (Figures S1 and S2) were performed at each temperature to obtain precise unit cell (Figure 1) and structural parameters (Figure 2 and deposited CIFs). As previously reported [28], CHA exhibits very strong negative thermal expansion (Table 1), which is measured over a significantly larger temperature range with a large number of data points in the present case (Figure 1; Figure S3). The maximum value of α_v was found to be $-2.50(5) \times 10^{-5}$ K^{-1} at 100 K. Contraction was found to be essentially isotropic.

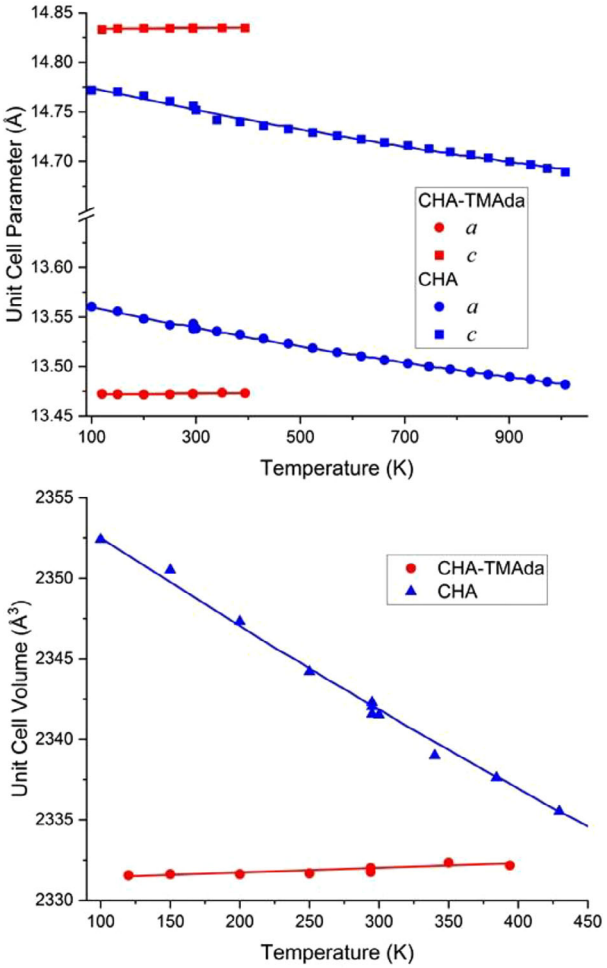

FIGURE 1 | Unit cell parameters and volumes of CHA-TMAda and CHA as functions of temperature.

The presence of TMAda in the *cha* cage of chabazite induces a strong distortion with an increase in its height and reduction in its diameter [30]. The presence of the charge compensating fluoride ions in the *d6r* produces only a slight decrease in its height (Figure 3). This results in an increase in the *c* lattice parameter, a decrease in *a* and in the unit cell volume. The structure collapses slightly to adapt to the shape of TMAda under the effect of the intermolecular interactions between the SiO_2 framework and the TMAda. The cell volume of CHA-TMAda was found to increase only by 0.02% over the 120–394 K temperature range with an α_v of $0.12(2) \times 10^{-5}$ K^{-1}. This value is one of the lowest measured for any material, particularly for single component materials rather than composites. In addition, the ZTE behavior is isotropic (Table 1).

In CHA, the *d6r* cage contracts more than the *cha* cage, in fact the diameter of the latter is stable over a large temperature range from 100–700 K followed by a slow decrease (Figure 3). In parallel, the Si—O2—Si angle, which is specific to the *cha* cage increases before becoming stable. This is compensated by the decrease followed by the stabilization of the Si—O1—Si angle. The contraction of

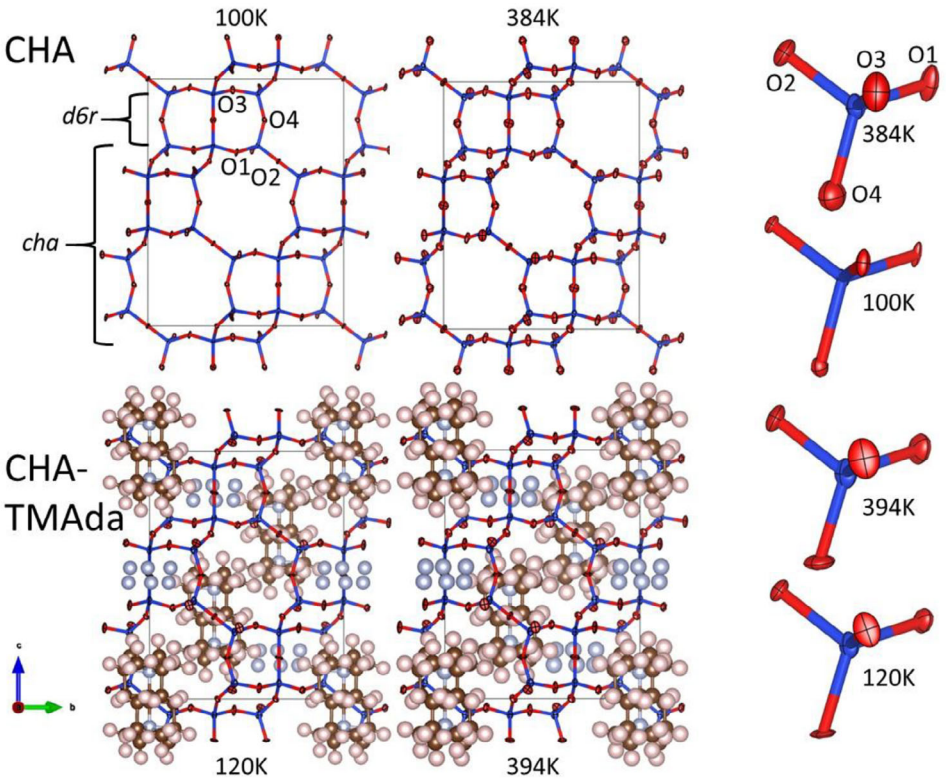

FIGURE 2 | Crystal structures (left) and enlarged individual SiO_4 tetrahedra (right) of CHA and CHA-TMAda at low and high temperature. Framework Si and O atoms are represented in blue and red, respectively. The extraframework atoms are represented in brown (C), light gray (N), light brown (H), and light blue (F). The TMAda and fluoride ions are disordered over 2 and 12 sites in the *cha* and *d6r* cages, respectively. ADP ellipsoids are plotted at 50% probability.

TABLE 1 | Unit cell parameters (Å), volume (Å^3), and thermal expansion coefficients α_0 ($\times 10^{-5}$ K^{-1}), α_1 ($\times 10^{-8}$ K^{-2}) for CHA and CHA-TMAda, $\alpha_T = \alpha_0 + \alpha_1(T\text{-}100)$ obtained from thermal equation of state fits to the XRPD data.

CHA								
a_{100K}	α_0	α_1	c_{100K}	α_0	α_1	V_{100K}	α_0	α_1
13.5392(3)	−0.84(2)	0.38(4)	14.7524(8)	−0.82(6)	0.4(1)	2352.5(2)	−2.50(5)	1.13(9)
CHA-TMAda (linear fit: $\alpha_1 = 0$)								
a_{100K}	α_0	α_1	c_{100K}	α_0	α_1	V_{100K}	α_0	α_1
13.4717(3)	0.04(1)	—	14.8339(3)	0.03(1)	—	2331.4(1)	0.12(2)	—

the *d6r* is also linked to the decrease in this latter angle along with that of the Si—O4—Si angle. It can be noted that the SiO_4 tetrahedra remain very stable with the O—Si—O angles remaining identical and the average, apparent Si—O distance decreasing by 0.008 Å over the 100–1008 K range (Table S1). In comparison with previous work [28, 29], the magnitudes of the changes in the Si—O—Si angles, the intratetrahedral distances, and angles are lower.

In CHA-TMAda, the change in height of both cages with temperature is almost negligeable. The remaining decrease in the diameter of the *d6r* cages is more than compensated by the increase in that of the *cha* cage. This is associated with a slight decrease in Si—O1—Si angle and an increase in the Si—O2—Si, while the Si—O3—Si and Si—O4—Si angles remain stable. The overall effect of the TMAda and the charge compensating fluoride ions is a much lower NTE for the *d6r* with very slight positive thermal expansion for *cha* cage. The F^- exerts a more pronounced effect proportionally concerning the small *d6r* cage; however, the effect of the TMAda on the much larger *cha* cages dominates in absolute terms in the overall modification to the thermal expansion as there are an equal number of each type of cage in the structure.

The present results can be analyzed in the framework of the AAV concept [22] (Table S2). Empty CHA has an AAV of 21.7 Å^3 and would be expected to exhibit NTE as observed experimentally. Taking into account the OSDA and the F^- ions, the AAV decreases to 10.4 Å^3 and PTE would be expected. Up to the present, the AAV concept [22] has not been applied to organic guest molecules.

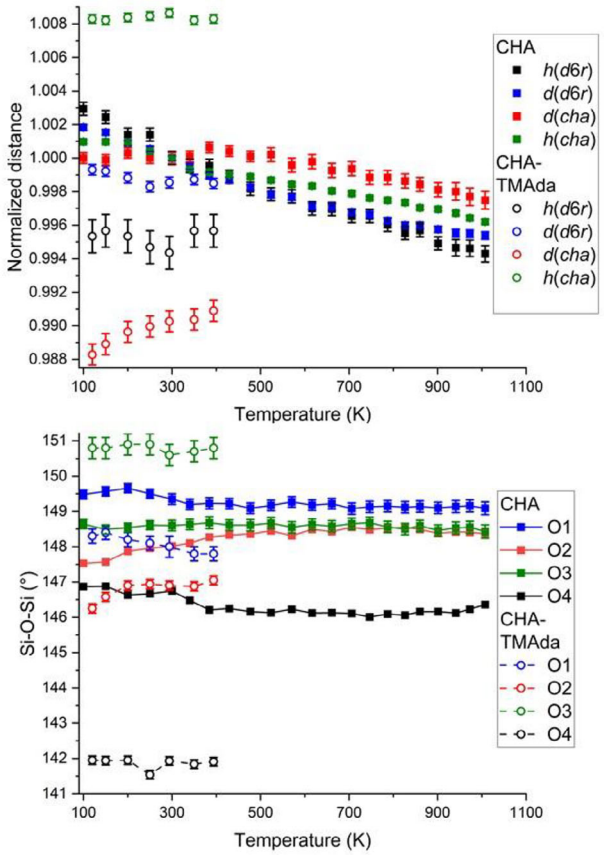

FIGURE 3 | Normalized height (h) and diameter (d) of *d6r* and *cha* cages and intertetrahedral Si—O—Si angles for CHA-TMAda and CHA as functions of temperature.

The hydrogen atoms in such molecules are distinct due to their small size and thus volume occupied in a crystal structure. Hydrogen atoms lie to a great extent inside the van der Waals radii of the carbon atoms to which they are bonded and thus their contribution is significantly lower than other larger atoms. If the hydrogen atoms are not considered, the AAV of CHA-TMAda would be 15.2 Å^3, which is very close to the limiting value of 16 Å^3 corresponding to ZTE.

The static changes in average distances and angles do not provide direct information on the mechanism of NTE in chabazite. A previous study based on the pair distribution function method [29] linked the mechanism to a thermally activated mode that translates along the Si—O3—Si—O4—Si linkages in the *d6r* resulting in a reduction in Si—Si distances. Information on such modes can be obtained from the atomic displacement parameters (ADP). The ADPs were refined anisotropically and from the equivalent isotropic ADP, U_{eq} (Figure 4; Figure S4), it can be seen that the values for the oxygen atoms in the *d6r* cage, O1, O3, and O4, increase to a greater extent than that of O2, which only is found in the *cha* cage. More importantly, analysis of the anisotropic ADPs has allowed the root mean square displacements (RMS) of the oxygen atoms along the principal axes of the ADP ellipsoids to be calculated and which are given in Table S3 at the low and high temperature limits for the comparison between CHA and CHA-TMAda. Typically, the increase in one transverse component dominates (Table S3; Figure 2) giving rise to a contribution to

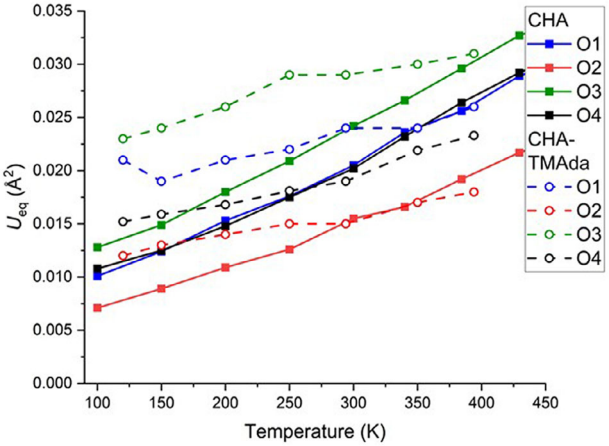

FIGURE 4 | Equivalent isotropic ADPs (U_{eq}) for CHA-TMAda and CHA as a function of temperature.

the overall NTE. These transverse displacements correspond to atomic motion essentially perpendicular to the Si-O-Si linkages in the framework.

Significant differences are observed for the ADPs for CHA-TMAda. Initially the silicon and oxygen U_{eq} values are slightly higher as there will also be a static component due to interactions between the oxygen and silicon atoms of the CHA framework and the disordered TMAda in the *cha* cages and the fluoride ions in the *d6r*. The thermally activated dynamic component increases at a much slower rate than for CHA giving a lower overall increase in *Ueq* for the silicon and all the oxygen atoms indicating that the phonon amplitudes are less activated by temperature. Strikingly, the increases in the transverse components of the RMS displacements of the oxygen atoms (Table S3) are in the range of 10%–33% from 120 to 394 K as opposed to 43%–117% from 100 to 384 K for CHA. This clearly shows the effect of the TMAda and fluoride ions on the transverse oxygen displacements linked to the NTE behavior of CHA, thereby resulting in ZTE in CHA-TMAda.

3 | Conclusion

In conclusion, the presence of OSDAs in the final structure of these host-guest materials, which direct the formation of zeolites during hydrothermal synthesis, can also tune the intrinsic thermal properties of porous zeolitic frameworks. The strength of the interactions between the OSDA and the framework (Coulomb electrostatic, van der Waals, CH…O hydrogen bond), that come into play for structure direction, also affects the atomic displacements of oxygen atoms and ultimately the overall thermal expansion properties. Herein, we have shown that starting from a zeolite framework like chabazite with strong intrinsic NTE properties and an OSDA, a new class of host-guest ZTE materials made of light, abundant, and non-toxic elements, can be obtained through a simple and straightforward strategy

4 | Experimental Section/Methods

CHA-TMAda was synthesized hydrothermally using tetraethyl orthosilicate (TEOS) as the silica source, N,N,N-Trimethyl-1-

adamantylammonium Hydroxide (TMAdaOH) as the organic structure directing agent (OSDA) in the presence of fluoride ions, and adapting a previous protocol [27] by the inclusion of seeds. In order to obtain siliceous chabazite CHA, the CHA-TMAda was calcined in air at 823 K to remove the OSDA. Details of the synthesis and sample characterization are presented in Supporting Information.

CHA-TMAda was studied by XRPD (λ = 0.67837 Å) in a 0.3 mm diameter glass capillary as a function of temperature from 120–394 K on the two-circle diffractometer equipped with a Dectris Mythen II detector at the CRISTAL beamline at the Synchrotron SOLEIL. XRPD measurements (λ = 0.35451 Å) from 100–1008 K on CHA (which had been calcined at 823 K) in 1 mm diameter quartz capillaries were performed on the two-circle diffractometer ID22 beamline [31] equipped with the multianalyzer [32] stage and a Dectris Eiger CdTe 2M-W detector at the European Synchrotron Radiation Facility. Full details of the XRPD measurements and structure refinements are given in the Supporting Information.

CCDC 2523560–2523588 contain the supplementary crystallographic data for this paper. These data can be obtained free of charge from The Cambridge Crystallographic Data Centre via www.ccdc.cam.ac.uk/data_request/cif.

Acknowledgements

The synchrotron x-ray diffraction experiments were performed at the CRISTAL beamline at the Synchrotron SOLEIL (proposal numbers: 20241654 and 20250009) and the ID22 beamline at the European Synchrotron Radiation Facility (HC-6300). We thank K. Ata for preliminary chabazite syntheses, M. Camblor for helpful discussions, and A. van der Lee for help with placing the H atoms in CHA-TMAda.

Open access publication funding provided by COUPERIN CY26.

Conflicts of Interest

The authors declare no conflicts of interest.

Data Availability Statement

XRPD data from the ESRF are available at https://doi.esrf.fr/10.15151/ESRF-ES-2227082660. All other data are available from the authors.

References

1. J. J. Shaffer and H. E. Bennett, "Effect of Thermal Cycling on Dimensional Stability of Zerodur and ULE," *Applied Optics* 23 (1984): 2852–2853, https://doi.org/10.1364/ao.23.002852.

2. J. S. O. Evans T. A. Mary, and A. W. Sleight, "Negative Thermal Expansion in a Large Molybdate and Tungstate family," *Journal of Solid State Chemistry* 133 (1997): 580–583, https://doi.org/10.1006/jssc.1997.7605.

3. P. Mohn, "A Century of Zero Expansion," *Nature* 400 (1999): 18–19, https://doi.org/10.1038/21778.

4. J. R. A. Davis, *Alloying: Understanding the Basics* (ASM International, 2001).

5. J. R. Salvador, F. Gu, T. Hogan, and M. G. Kanatzidis, "Zero Thermal Expansion in YbGaGe due to an Electronic Valence Transition," *Nature* 425 (2003): 702–705, https://doi.org/10.1038/nature02011.

6. A. Sleight, "Zero-Expansion Plan," *Nature* 425 (2003): 674–676, https://doi.org/10.1038/425674a.

7. T. Suzuki and A. Omote, "Zero Thermal Expansion in $(Al_{2x}(HfMg)_{1-X})(WO_4)_3$," *Journal of the American Ceramic Society* 89 (2006): 691–693, https://doi.org/10.1111/j.1551-2916.2005.00729.x.

8. K. Takenaka and H. Takagi, "Zero Thermal Expansion in a Pure-Form Antiperovskite Manganese Nitride," *Applied Physics Letters* 94 (2009): 131904, https://doi.org/10.1063/1.3110046.

9. K. Takenaka, "Negative Thermal Expansion Materials: Technological Key for Control of Thermal Expansion," *Science and Technology of Advanced Materials* 13 (2012): 013001, https://doi.org/10.1088/1468-6996/13/1/013001.

10. L. Hu, J. Chen, L. L. Fan, et al., "Zero Thermal Expansion and Ferromagnetism in Cubic $Sc_{1-x}M_XF_3$ (M = Ga, Fe) over a Wide Temperature Range," *Journal of the American Chemical Society* 136 (2014): 13566–13569, https://doi.org/10.1021/ja5077487.

11. J. L. Xu, L. Hu, Y. Z. Song, et al., "Zero Thermal Expansion in Cubic $MgZrF_6$," *Journal of the American Ceramic Society* 100 (2017): 5385–5388, https://doi.org/10.1111/jace.15105.

12. S. P. Li, R. J. Huang, Y. Q. Zhao, W. Wang, Y. M. Han, and L. F. Li, "Zero Thermal Expansion Achieved by an Electrolytic Hydriding Method in $La(Fe,Si)_{13}$ Compounds," *Advanced Functional Materials* 27 (2017): 1604195, https://doi.org/10.1002/adfm.201604195.

13. M. J. Xia, F. Liang, X. H. Meng, Y. G. Wang, and Z. S. Lin, "Intrinsic Zero Thermal Expansion in Cube Cyanurate $K_6Cd_3(C_3N_3O_3)_4$," *Inorganic Chemistry Frontiers* 6 (2019): 2291–2295, https://doi.org/10.1039/c9qi00709a.

14. N. K. Shi, A. Sanson, A. Venier, et al., "Negative and Zero Thermal Expansion in α-$(Cu_{2-x}Zn_x)V_2O_7$ Solid Solutions," *Chemical Communications* 56 (2020): 10666–10669, https://doi.org/10.1039/d0cc04505e.

15. J. N. Liu, H. E. Maynard-Casely, H. E. A. Brand, and N. Sharma, "$Sc_{1.5}Al_{0.5}W_3O_{12}$ Exhibits Zero Thermal Expansion between 4 and 1400 K," *Chemistry of Materials* 33 (2021): 3823–3831, https://doi.org/10.1021/acs.chemmater.1c01007.

16. B. A. Marinkovic, P. I. Ponton, C. P. Romao, T. Moreira, and M. A. White, "Negative and near-Zero Thermal Expansion in $A_2M_3O_{12}$ and Related Ceramic Families: a Review," *Frontiers in Materials* 8 (2021): 741560, https://doi.org/10.3389/fmats.2021.741560.

17. Y. Zheng, Y. X. Jiao, Y. Q. Qiao, et al., "Control of Thermal Expansion in $TaVO_5$ by Double Chemical Substitution," *Inorganic Chemistry* 62 (2023): 8543–8550, https://doi.org/10.1021/acs.inorgchem.3c00090.

18. Y. M. Xiang, Y. M. Zhang, X. S. Liu, et al., "Tailoring Thermal Expansion of β-$Cu_2V_2O_7$ with Improved Mechanical Properties by Incorporation of Li^+Fe^{3+}," *Ceramics International* 50 (2024): 53790–53794, https://doi.org/10.1016/j.ceramint.2024.10.232.

19. J. C. Luo, K. X. Zou, B. Wang, et al., "Zero Thermal Expansion Behavior in High-Entropy Anti-Perovskite $Mn_3Fe_{0.2}Co_{0.2}Ni_{0.2}Mn_{0.2}Cu_{0.2}N$," *Advanced Functional Materials* 34 (2024): 2106108, https://doi.org/10.1002/adfm.202410608.

20. Y. Z. Song, J. M. Zhang, C. Zhou, N. K. Shi, and J. Chen, "Research Progress on Zero Thermal Expansion Metallic Materials," *Acta Metallurgica Sinica* 61 (2025): 00264, 10.11900/0412.1961.2024.00264.

21. Q. J. Wang, Y. Q. Qiao, K. Y. Zhao, et al., "Zero Thermal Expansion in K_x Mn_x $in_{2-x}(MoO_4)_3$ Based Materials," *Acta Materialia* 281 (2024): 120358, https://doi.org/10.1016/j.actamat.2024.120358.

22. Q. L. Gao, J. Q. Wang, A. Sanson, et al., "Discovering Large Isotropic Negative Thermal Expansion in Framework Compound $AgB(CN)_4$ via the Concept of Average Atomic Volume," *Journal of the American Chemical Society* 142 (2020): 6935–6939, https://doi.org/10.1021/jacs.0c02188.

23. M. P. Attfield and A. W. Sleight, "Exceptional Negative Thermal Expansion in $AlPO_4$-17," *Chemistry of Materials* 10 (1998): 2013–2019, https://doi.org/10.1021/cm9801587.

24. M. Ducamp and F. X. Coudert, "Systematic Study of the Thermal Properties of Zeolitic Frameworks," *The Journal of Physical Chemistry C* 125 (2021): 15647–15658, https://doi.org/10.1021/acs.jpcc.1c03975.

25. F. Y. Qin, X. Y. Bai, Y. W. Fang, et al., "Giant Negative Thermal Expansion Exceeding 1000 K in $PrMnO_3$ via Synergy of Local Structure Distortion and Orbital Disordering," *Nature Communications* 16 (2025): 9977, https://doi.org/10.1038/s41467-025-64925-7.

26. F. Alabarse, B. Baptiste, B. Joseph, and J. Haines, "Tuning Negative Thermal Expansion in $AlPO_4$-17 by Insertion of Guest Molecules," *The Journal of Physical Chemistry Letters* 13 (2022): 9390–9395.

27. M. J. Díaz-Cabañas, P. A. Barrett, and M. A. Camblor, "Synthesis and Structure of Pure SiO_2 Chabazite: the SiO_2 Polymorph with the Lowest Framework Density," *Chemical Communications* 17 (1998): 1881–1882.

28. D. A. Woodcock, P. Lightfoot, L. A. Villaescusa, M. J. Díaz-Cabañas, M. A. Camblor, and D. Engberg, "Negative Thermal Expansion in the Siliceous Zeolites Chabazite and ITQ-4: a Neutron Powder Diffraction Study," *Chemistry of Materials* 11 (1999): 2508–2514.

29. M. M. Martínez-Iñesta and R. F. Lobo, "Investigation of the Negative Thermal Expansion Mechanism of Zeolite Chabazite Using the Pair Distribution Function Method," *The Journal of Physical Chemistry B* 109 (2005): 9389–9396, https://doi.org/10.1021/jp044165w.

30. L. A. Villaescusa, I. Bull, P. S. Wheatley, P. Lightfoot, and R. E. Morris, "The Location of Fluoride and Organic Guests in 'as-made' Pure Silica Zeolites FER and CHA," *Journal of Materials Chemistry* 13 (2003): 1978–1982, https://doi.org/10.1039/b300728f.

31. A. Fitch, C. Dejoie, E. Covacci, et al., "ID22 – the High-Resolution Powder-Diffraction Beamline at ESRF," *Journal of Synchrotron Radiation* 30 (2023): 1003–1012, https://doi.org/10.1107/s1600577523004915.

32. J. L. Hodeau, P. Bordet, M. Anne, et al., "Nine Crystal Multi-Analyser Stage for High Resolution Powder Diffraction between 6 and 40 keV," in *Conference on Crystal and Multilayer Optics*, (SPIE, 1998), 353–361, https://doi.org/10.1117/12.332525.

Supporting Information

Additional supporting information can be found online in the Supporting Information section.

Supporting File: adfm75257-sup-0001-SuppMat.pdf.